Automatic Optical Inspection of Solder Ball Burn Defects on Head Gimbal Assembly

Jirarat Ieamsaard, Paisarn Muneesawang and Frode Eika Sandnes

***Abstract*— The detection of low quality solder joint quality in hard disk drive (HDD) manufacturing is a time consuming, error-prone and costly process that is often performed manually. This paper thus proposes two automated optical solder jet ball joint defect inspection methods for head gimbal assembly (HGA) production. The first method uses a Support Vector Machine (SVM) for fault detection and the second method uses vertical edge detection to identify solder ball and pad burning defects. The methods were tested with 5,530 HGA images, and their performance was compared to a Bayesian-based method. Experimental results show that the vertical edge detection method gave the best results, with an under reject rate of 0.75% and an over reject rate of 1.88%. The accuracy of the vertical edge detection method was 98.2%, which is higher than the accuracy of 89.9% for the Bayesian-based method, and 84.6% for the SVM-based method.**

***Index Terms*— optical inspection; solder jet ball joint defect; vertical edge detection; HDD manufacture**

I. Introduction

The amount of digital information is believed to have grown rapidly during the last decades. It has been estimated that hard disk drives (HDDs) account for 52% of this information [1] and the HDD market is expected to grow further [2]. The HDD data storage density has increased dramatically while the physical HDD size has shrunk. A typical 2.5 inch form factor HDD is 69.85 mm wide, 100 mm deep, and 9.5 mm high [3].

Product output is often increased to meet the demands of the HDD market. This is achieved by improving the automatic or semi-automated HDD production line for each sub-process. One of the semi-automated production lines builds the Head Gimbals Assembly (HGA) which is a key component of the read/write part of a HDD. A HGA consists of a slider and a suspension mechanism. Mistakes that cause defects occur when solder jet bond (SJB) machines are used to assemble the slider and suspension mechanisms. Fig. 1 shows an example of a solder ball burning defect.

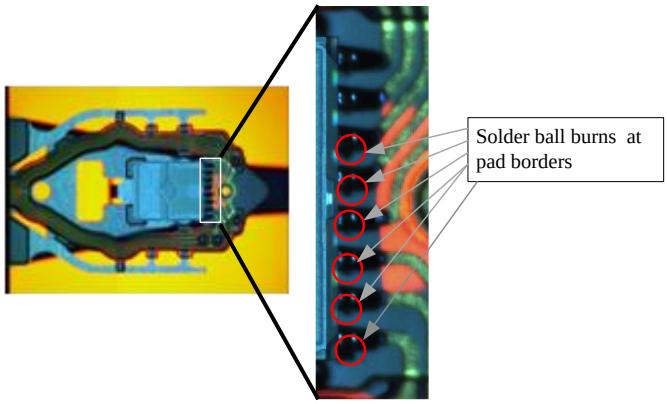

Fig. 1. Example HGA solder ball burnt defect.

In the HGA production line that was the subject of this study, the SJB machine first connects the suspension circuit to the slider body. Then, the HGA is placed on pallets and transferred via a conveyor belt to a Visual Inspection and OCR Reading (VOR) machine. Nine cameras take photos for defect analysis. First, two cameras on the left and right side take two on-the-fly shots. Next, the remaining seven cameras capturing various angles that are triggered simultaneously. The VOR employs COGNEX for automatic vision processing. HGA images are processed to detect HGA defects and the results are sent to the module controller. The inspection system is shown in Fig 2.

The COGNEX typically results in a high false positive rate. Therefore, the many HGAs that are flagged as defect by COGNEX are therefore inspected manually using microscopes with 40x magnification. Manual inspection occasionally fails to detect defects. Inspectors may experience fatigue, the skill and experience of the inspectors vary, and it is challenging to control environmental factors such as lighting conditions. The motivation of this study was therefore to develop an automated visual inspection procedure to achieve higher reliability, faster fault detection and lower production costs.

This paragraph of the first footnote will contain the date on which you submitted your paper for review. It will also contain support information, including sponsor and financial support acknowledgment. For example, "This work was supported in part by the U.S. Department of Commerce under Grant BS123456".

The next few paragraphs should contain the authors' current affiliations, including current address and e-mail. For example, F. A. Author is with the National Institute of Standards and Technology, Boulder, CO 80305 USA (e-mail: author@ boulder.nist.gov).

S. B. Author, Jr., was with Rice University, Houston, TX 77005 USA. He is now with the Department of Physics, Colorado State University, Fort Collins, CO 80523 USA (e-mail: author@lamar.colostate.edu).

T. C. Author is with the Electrical Engineering Department, University of Colorado, Boulder, CO 80309 USA, on leave from the National Research Institute for Metals, Tsukuba, Japan (e-mail: author@nrim.go.jp).

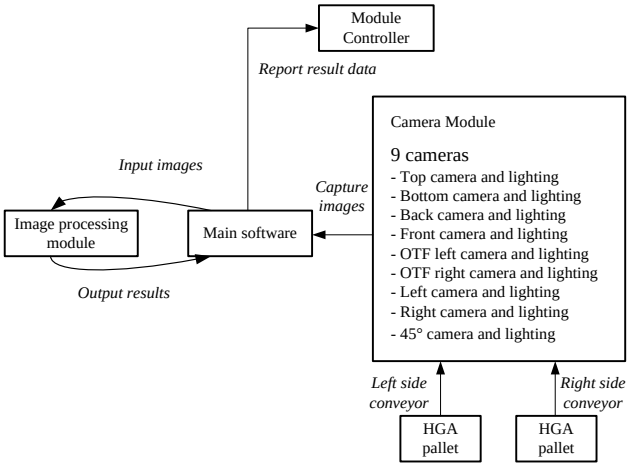

Fig. 2. HGA visual inspection system

This study focuses on the potential defects in the solder joint between the slider and the suspension mechanism caused by errors in the soldering process using the solder jet bounding (SJB) machine. Errors occur at the point where the solder balls and the melting pad area meet. Defect characteristics include uneven pad edges or black traces along pad borders.

This paper is organized as follows; related work is described in Section II, the proposed support vector machine and vertical edge detection method is described in Section III, experimental results is provided in Section IV, and limitation of this study in Section V. Finally, Section VI concludes the paper.

II. Related Work

A. Previous work

There is a vast body of research into detecting semiconductor defects in general. Shankar et al. [24] described a vision-based system to detect defect on semiconductors. They applied subtractive correlation for matching reference images and test images. Morhphological operators were also used to identify defects. Their method successfully detected chip out, bridging, and scratched regions on semiconductor wafer surfaces. Zontak and Cohen [25] described a reference-based method for wafer defect detection using anisotropic kernel reconstruction of the source image from the reference image. Tsai and Luo [26] used mean shift to detect human fingerprints and contaminations on multicrystalline solar wafers. Gray scale wafer images were converted into entropy images and then mean shift filtering was applied to remove noise and preserve the defective pixels in the filtered images. Yuan et al. [27] proposed a multistep semiconductor wafer defection procedure comprising defect denoising, defect clustering, pattern identification and finally fine-tuning. A more detailed description of related work on semiconductor inspection can be found in Hung and Pan's [23] recent survey.

Comparatively, there are fewer documented studies on the specific problem of HGA jet bonding defect detection. Ieamsaard and Fuangpian [4] proposed a visual inspection system using morphology and template matching for solder ball bridging ball defect detection and solder ball incomplete defect detection and compared the results to those obtained using a chain-code descriptor-based method. The morphology and template matching method provided 99.0% accuracy for both solder ball bridging and solder ball incomplete defect detection, respectively. The chain-code descriptor-based method provided an accuracy of 88.4% for solder bridging detection and 85.6% for solder ball incomplete detection. K-mean clustering was used for missing solder ball defect detection [4] to detect the contour of each pad. The complete contours forming loops were counted and finally classified. The method achieved a high accuracy of 99.6%. A Sobel-based vertical edge detection approach was also proposed for solder ball burning defects detection [4]. However, the performance of the Sobel-based method depends on the quality of the test image as false detections are easily caused by reflections due to the illumination.

Mak et al. [3] proposed a Bayesian approach to inspect solder jet balls in the HGA process, using Tree Augmented Naïve Bayes Network (TAN-BN) plus check classifier. The regions of interest and statistical features are used to describe the differences between good and bad solder balls. The Bayesian approach yielded an accuracy of 91.52% for classifying solder joints into the defect and non-defect groups.

Kunakornvung et al. [19] detected the presence of contamination on the Air Bearing Surface (ABS) of the slider using texture characteristics. Fak-aim et al, [20] proposed a system to inspect the completeness of soldering joints in X-Ray images of Flip-Chip components. They used a Genetic Algorithms (GA) to detect the edges of solder joints and compared their results with those obtained with the conventional Sobel and Canny edge detection methods. GAs provided the highest corrective percentage compared to Sobel and Canny. Withayachumnankul et al. [12] designed a filter kernel to detect hairline crack defect edges on the surface of hard disk amplified piezoelectric (PZT) actuators. The kernel filter detected lines at multiple angles. Chow et al.[21] presented a detection system for defects on HDD media surfaces using spectral imaging. They proposed thresholding and connecting-components labeling method and compared the results with results obtained using a mean-shift clustering method. The thresholding and connecting-components labeling was found to be a suitable method for media inspection. Gulphanich et al. [22] proposed a 3D object measurement and inspection system for measuring the hard drive dimensions (width and length) and for checking the tighten screw on the HDD assembly. HDD images were acquired using laser lighting sectioning, and these laser strip profiles were used to extract the object coordinates to determine the object size and screw defect.

III. Method

Two approaches to defect detection are proposed herein, the first uses based on a support vector machine to classify solder balls and the second uses vertical edge detection to identify

critical features. The two methods are also compared to the Bayesian based method introduced by Mak et al. [3].

A. *Bayesian based method*

In our adaptation of Mak et al.'s approach [3], the region of interest (ROI) containing the solder balls were segmented into 45×420 pixel sub-images from the 2400×2000 pixel HGA top view image. Sub-images were binarized using Otsu's method [5]. Each binary sub-image contained eight pads, and each of these pads were segmented into a 45×50 pixel area. The following statistical features were measured for each pad:

1) Size; the area of the detected object in the pad area.
2) Length; the perimeter of detected objects.
3) Shape; length squared divided by area.
4) Aspect ratio; the ratio of height of objects detected in the pad area; (height / width) × 100
5) Relative size; the ratio of bounded area. (height × width)/ (45×50) ×100.
6) Area ratio; the ratio of area of objects. (Size)/ (45×50) ×100.
7) Elements; the number of objects detected within the pad area.

Fig 3 shows example features for both a burnt pad and non-defective pads. The features were used as classifiers in the Bayesian classification process.

Elements	Size	Length	Shape	Aspect Ratio	Area Ratio	Relative Size	
1	1366	149.9	16.5	67.8	60.7	81.4	Non-defective
1	1330	148.5	16.6	66.1	59.1	79.5	Non-defective
1	1333	147.0	16.2	68.2	59.2	79.2	Non-defective
1	1335	147.6	16.3	66.6	59.3	79.4	Non-defective
1	1320	148.0	16.6	65.8	58.7	78.6	Non-defective
1	1343	147.9	16.3	67.2	59.7	80.0	Non-defective
1	1342	148.0	16.3	66.9	59.6	80.0	Non-defective
1	1487	176.0	20.8	77.4	66.1	100.4	**Burnt pad**

Fig. 3 Example non-defective and burnt pad features.

Bayesian classifiers can be used when the predictors of each class are independent. Data is classified using training data by estimating the parameters of a probability distribution assuming predictors for the class are conditionally independent. The posterior probability is computed for any unseen test data that belong to each class. The class that has the highest probability is declared the 'winner' and is assigned the class label for that combination of evidence. The posterior probability distribution of $P(X \mid Y = y)$ is given by Bayes' rule

$$P(X \mid Y = y) = \frac{P(Y = y \mid X)P(X)}{P(Y = y)}$$

Where $P(Y = y \mid X)$ is the likelihood that the probability of predictor given class, $P(X)$ is the prior probability of the class, and $P(Y = y)$ is the prior probability of the predictor. A Bayesian classifier with a Kernel distribution was applied to the classification of solder joints as non-defective or defective.

A total of 94 burnt pads and 800 non-defective pads were collected to find the close-to-optimal number of training samples. The training size was set according to the condition $\eta = e_1 < 1\%$ where η is the number of training samples and e_1 is the under reject rate. In order to determine the optimal training parameters the number of burnt pads were varied from 10 to 94 (in steps of 10), while the number of non-defective pads were varied from 30 to 800 in increasing steps of 20, 30 and 100. For each configuration the Bayesian-based method was executed and the over and under reject rates were recorded.

The under reject was less than 1% with 50 to 100 non-defective pads and 66 to 94 defective pads. Fig. 10 shows the result of setting the number of defective pads to 70%, 80%, 90% and 100% with 100 non-defective pads, while Fig. 11 shows that the under reject rate was less than 1% with 50-100 non-defective pads in the training set. Fig. 12 shows that the accuracy and precision are low when the under reject rate is less than 1%. Based on these observations a training set with 66 burnt pads and 800 non-defective pads was used in the experiments as these parameters provide the highest accuracy.

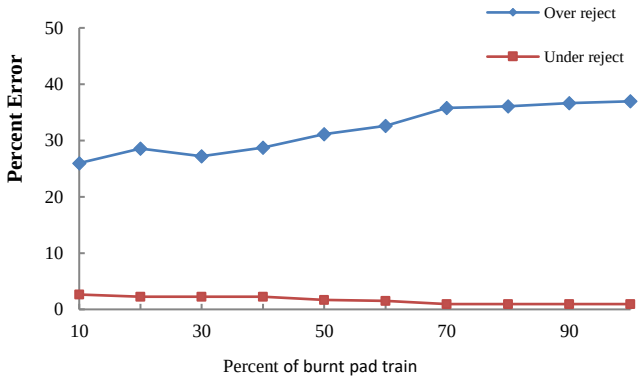

Fig 10. The over reject rates and under reject rates for different defective pad training set sizes.

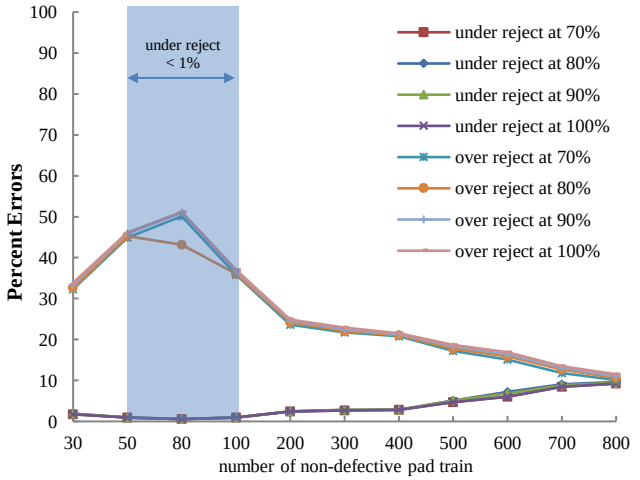

Fig 11. The over reject rates and under reject rates for different non-defective pad training set sizes.

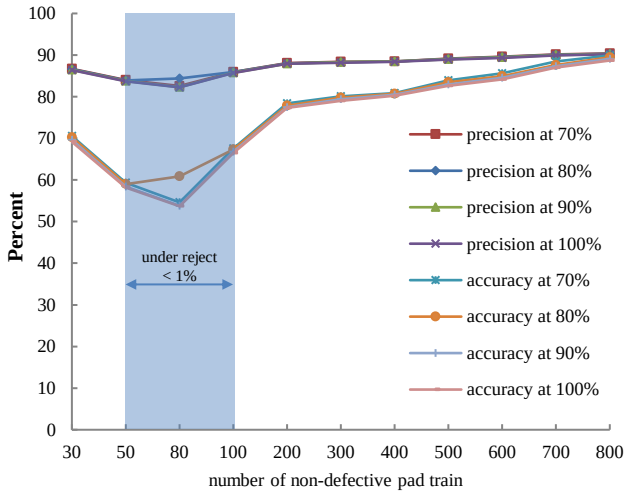

Fig 12. Precision and accuracy for different non-defective pad training set sizes.

B. *Support vector machine based method*

Support vector machines are supervised learning models that are commonly used for classification tasks [15-17]. SVMs are capable of performing both linear and effective non-linear classification using the kernel trick in high dimensional space. This study set out to explore the suitability of support vector machines for classifying defect versus non-defect pads.

After the ROI was segmented the region-based and statistical features were extracted including size, length, shape, aspect ratio, relative size, area ratio, and the number of objects detected in the pad area. The SVM uses these features to classify pads as non-defective or defective. Given a set of training samples, the SVM training algorithm builds a model that assigns new examples into one of the two categories. A radial basis function (RBF) kernel was used as it yields a high performance in term of accuracy compared to others kernels. The RBF kernel is defined as [15]

$$K(x_i, x_j) = \exp(-\frac{\|x_i - x_j\|}{2\sigma^2})$$

where x_i and x_j are samples, and $\sigma > 0$ is a constant that defines the kernel width. The optimal kernel function parameter σ was found experimentally to be 0.4.

In order to determine the optimal training parameters the number of burnt pads were varied from 10 to 94 (in steps of 10), while the number of non-defective pads were varied from 30 to 800 in increasing steps of 20, 30 and 100. For each configuration the Support Vector Machine-based method was executed and the over and under reject rates were recorded.

The under reject was less than 1% with 30 to 200 non-defective pads and 18 or more defective pads. Fig. 13 shows the effects of varying the number of defective with 100 non-defective pads. The lowest under reject rate of 0.37% was achieved with 90% of the 94 defective pads in the training set. The over reject rate was low when the non-defective training set size was large. The precision and accuracy were low when the under reject rate was less than 1% as show in Fig 14. The precision and accuracy were greater than 80% when the over reject rate was about 4% and the under reject rate was about 16%. Consequently, a training set with 85 burnt pads and 800 non-defective pads were chosen for the training set in this experiment since these parameters provide the highest accuracy.

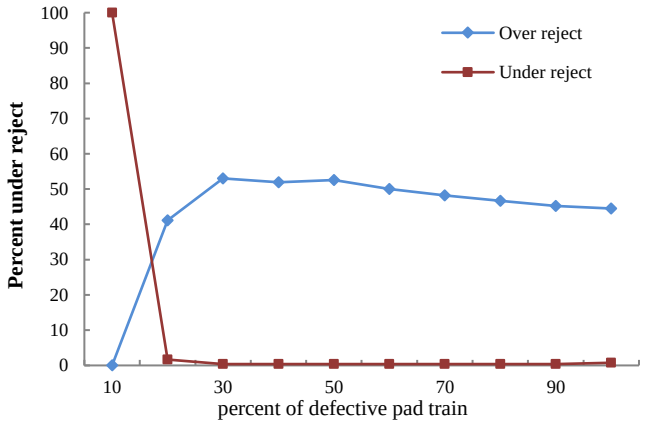

Fig 13. The over reject rates and under reject rates for different defective pad training set sizes.

.

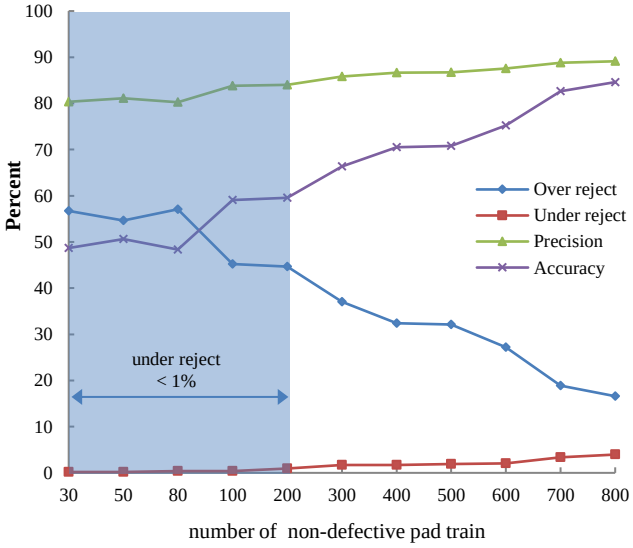

Fig 14. The over reject rate, under reject rate, precision, and accuracy for non-defective pad training set sizes.

C. *Vertical edge detection based method*

Burnt pads are characterized by uneven pad edges, or black limbs around the border, whereas non-defective pads have smooth borders. The difference between a non-defective pad and a defective pad is clearly visible from the vertical edge. Hence, the proposed method uses vertical edge detection. The overall algorithm is shown in Fig. 4.

Input: *Original HGA Image*
1. ***Pre-Processing***
Segment ROI from *Original HGA Image* using cross correlation
Make binary *sub-image* using Otsu's method.

2. ***Detect reflection***
Use circular Hough transform to detect reflection area.

3. ***Vertical edge analyze***
Apply the VEDA to detect vertical edge.
Remove vertical edge due to reflection.

4. ***Calculate pad area***
Calculate area of each pad in the binary sub-image

5. ***Make decision***
If (summation of edge pixels > decision value
pad area > area threshold)
Result = defect found.
Else
Result = non-defective.
End If

Fig. 4. The proposed method

The algorithm begins with ROI segmentation; the solder joint region of interest is extracted by cross correlation [6], [7]. The 2400×2000 pixel HGA images are correlated with the 45×420 pixel template image. A reference point is thus found where the correspondence between the input image and the template image is the highest. Using the reference point, the region of interest is extracted as a sub image of size 45 × 420 pixels. Next, the solder sub image is binarized using Otsu's method [5]. The threshold is selected such that the reparability of the gray level classes is maximized. The procedure utilizes only the zeroth and the first order cumulative moments of the gray level histogram. Otsu's method exhaustively searches for the threshold that minimizes the within-class variance, defined as a weighted sum of variances,

$$\sigma^2_{within}(t) = \omega_1(t)\sigma_1^2(t) + \omega_2(t)\sigma_2^2(t) \quad (2)$$

Here, ω_i are the probabilities of the two classes separated by a threshold *t* and variances σ_i^2 of the classes.

The pads contain white circles caused by light reflections. These reflections cause unwanted vertical edges on the pads in the subsequent edge detection step, and should be removed to increase solder defect detection accuracy. The reflections are detected using the circular Hough transform [8] where a cricle is represented using:

$$r^2 = (x-a)^2 + (y-b)^2 \quad (3)$$

Here *a* and *b* is the circle center coordinate and *r* is the circle radius. The parametric representation of this circle is:

$$x = a + r\cos(\theta) \quad (4)$$
$$y = b + r\sin(\theta) \quad (5)$$

If the angle θ *is* swept through a full 360 degree rotation, the points *(x, y)* trace the circle perimeter. If an image contains points that fall on circle perimeters, the task is to find parameter triplets *(a, b, R)* to describe each circle. The locus of *(a, b)* points in the parameter space fall on a circle of radius R centered at *(x, y)*. The true center point will be common to all parameter circles, and is found using a Hough accumulation array [8]-[11].

Al-Ghaili et al. [13]-[14] proposed a vertical edge detection algorithm (VEDA) for license plate detection. Their results showed that VEDA has very high accuracy and is about nine times faster than the Sobel operator. It was therefore used in this study to detect vertical edges of burnt pad defects. VEDA concentrates on intersections of black–white and white–black pixels, by moving a 2x4 mask from left to right and from right to left, as described in Fig. 5.

Input: *Binary Image*
Create a white blank image as *Image(i,j);*
For every pixel in *Binary Image*
center=True; left=True; right=True;
If (all center mask values are *black*)
center=False;
End If
If (all right mask values are *black*)
right=False;
End If
If (all left mask values are *black*)
left=False;
End If
If (!*center AND !right AND !left)*
Image(i,j)=white;
Image(i,j+1)=black;
End If
End For

Fig. 5. VEDA

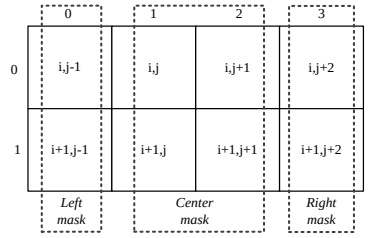

Fig. 6. A 2x4 window mask.

This process locates the black–white and white-black regions, and the 2x4 mask ensures that one- and two-pixel thick edges of each pad are detected. VEDA is about nine times faster than Sobel [15]-[16]. An example of applying VEDA is shown in Fig 7. The image is rotated for presentation purposes.

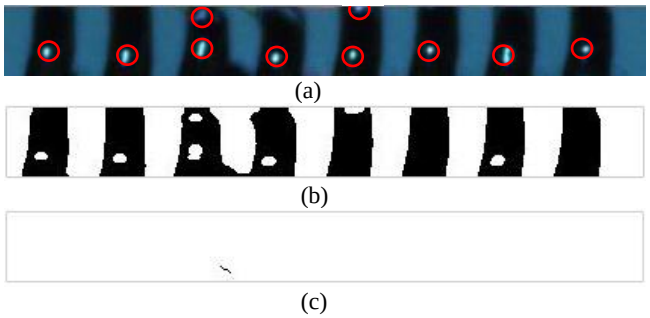

(a)

(b)

(c)

Fig 7. VEDA example: (a) RGB sub-image with red circle of reflection detected, (b) binary sub-image, (c) vertical edge of burnt pad

In order to reduce errors, the vertical edge caused by reflections within the pad is removed by checking for white pixels. If white pixels occur in the area of reflection, the pixels

are set to black.

$$I(x,y) = \begin{cases} 255 & \text{if } (x,y) \text{ is on the reflection area} \\ I(x,y) & \text{otherwise} \end{cases} \quad (6)$$

Yammen and Muneesawang used an area-based feature to identify corrosion on the pole tip on the HGA actuator component [6]. In this work, a similar area-based feature was applied to detect burnt pads whose burn area covers the entire pad from bottom to top, but has no vertical burnt pad edges. If the pad area is greater than a threshold T a defect is found. The pad area threshold is obtained from:

$$T = \left(\frac{Area\ of\ ROI}{Number\ of\ pads}\right) \times \frac{80}{100} \quad (7)$$

The 80/100 ratio is the percent of solder area covered on a pad. An experiment was conducted to obtain the optimal ratio that minimizes the sum of error percentages as shown in Fig. 8.

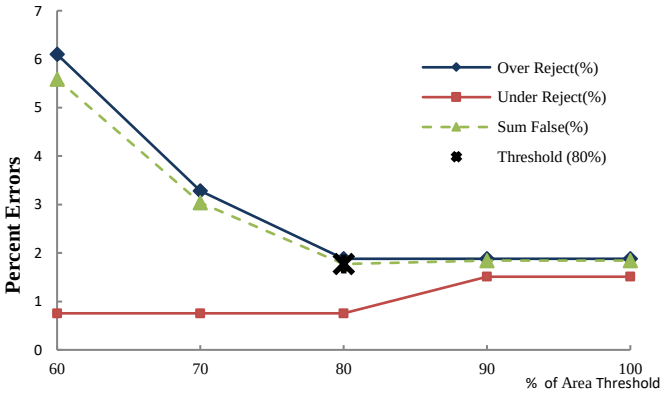

Fig 8. Finding the optimal ratio for the threshold T.

Finally, the algorithm decides whether a defect has been found or not. To make a decision, a vertical edge value (VE) is found by counting the black pixels in the pad image resulting from the previous steps. If VE is greater than a vertical edge threshold (VT) or the pad area is greater than the pad's threshold, a defect is found; otherwise no defect is detected.

The edge threshold (VT) was obtained experimentally. A threshold of 4 minimized the sum of error percentages as shown in Fig. 9.

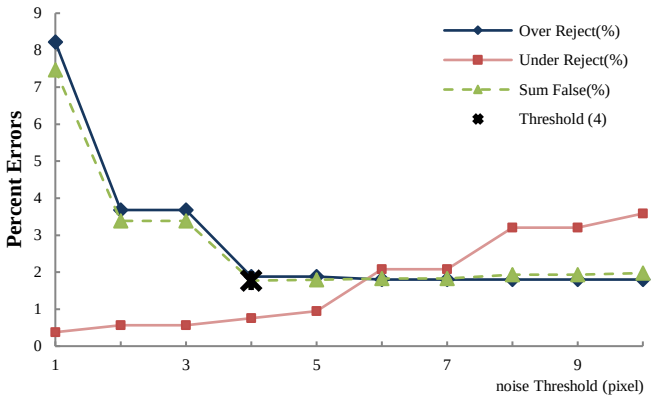

Fig 9. Edge threshold selection.

The output image of the vertical edge detection based method are shown in Fig 10, where indices Fig 10 a) – e) represent non-defective test images and indices Fig 10 f) – j) represent defective test images. The image are rotated for presentation purposes.

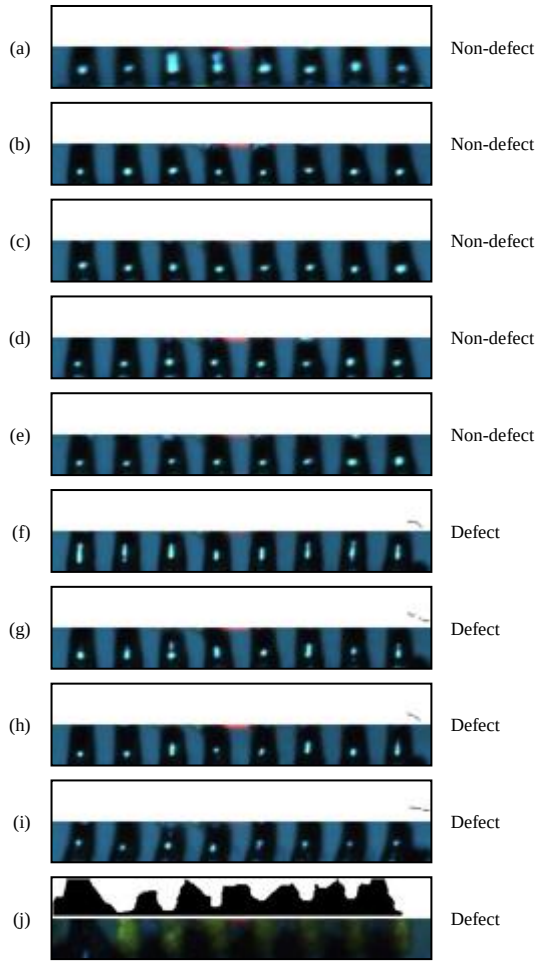

Fig 10. Output image for the proposed method (a) – (e) non-defective test image, (f) – (j) Defective test image

IV. EXPERIMENTAL RESULTS

The Bayesian-based method, the SVM-based method and

the vertical edge-based method were compared in the experiments. The test comprised 5,000 non-defective HGA images and 530 defective HGA images. The 2400 × 2000 pixel RGB images, with a resolution of 96 dpi were acquired using a mechanical camera positioning tool. A HGA was classified as defective if at least one of its eight pad edges was not smooth or its border had a black limb.

False detection is a key issue in the HDD industry and the methods were compared using the over reject rate and under reject rate. The over reject rate is the proportion of false detection of non-defective samples. The under reject rate is the portion of defective samples that goes undetected. In addition, the performance evaluation measurements, sensitivity, specification, precision, and accuracy were measured.

The training set that achieved the highest accuracy was chosen for Bayesian and SVM-based methods, namely 70% of the 94 burnt pads and 800 non-defective pads for Bayesian-based method, and 90% of the 94 burnt pads and 800 non-defective pads for SVM-based method.

The three methods were tested using the 5,000 non-defective and 530 defective HGA images in terms of over reject rates and under reject rates. The proposed vertical edge-based method yielded both the lowest over reject rate and the lowest under reject rate of 1.88% and 0.75%, respectively. The performance of the three method were compared using sensitivity (true positive rate), specificity (true negative rate), precision, and accuracy [18]. The proposed method achieved an accuracy of 98.2% while the Bayesian and SVM-based methods achieved accuracies of just 89.9% and 84.6%, respectively. The proposed vertical edge method also achieved high sensitivity, specificity and precision with 98.1%, 99.3%, and 99.9%, respectively, while, the Bayesian-based method achieved a sensitivity of 89.9%, specificity of 90.0%, and precision of 90.4 %. The SVM-based achieved an accuracy of 83.4%, a specification of 96.0%, and a 89.1% precision.

TABLE II
OVER REJECT RATES, UNDER REJECT RATES AND PERFORMANCE MEASUREMENTS

	Bayesian		SVM		Our method	
Over Reject						
non-defective: 5,000 images	505	10.10%	830	16.6%	94	1.88%
Under Reject						
defective : 530 images	53	10.00%	21	3.96%	4	0.75%
Performance Evaluation						
Sensitivity (true positive rate)	89.9 %		83.4 %		98.1 %	
Specificity (true negative rate)	90.0 %		96.0 %		99.3 %	
Precision	90.4 %		89.1 %		99.9 %	
Accuracy	89.9 %		84.6 %		98.2 %	

V. LIMITATIONS OF THIS STUDY

The experiments are based on test images stored in the jpeg format that relies on lossy compression and some vital image details might therefore have been lost. Some false detections were caused by the quality of the test image. The Bayesian-based method and the SVM-based method were particularly vulnerable since they use the shape feature to classify non-defective pads and burnt pads. Some non-defective pads were mistaken as small burnt pad shapes as their feature parameters are almost the same. However, the inspection system in production uses raw image and the real-world performance is therefore likely to be better than what was achieved in this study.

VI. CONCLUSION

A vertical edge detection method and a support vector machine-based method were proposed for the detection of HGA solder joints with ball or pad burns. Experimental results confirm the effectiveness of the vertical edge detection method, which outperforms both the Bayesian-based method and the SVM-based method.

The under reject rate is a key concern in HGA production lines and must according to the manufacturers be below 1%. The proposed method achieves a reject rate of 0.75%. Under reject rates of less than 1% were also achieved with the Bayesian and SVM based methods where the precision and accuracy decreased as a function of increasing over reject rates. Clearly, the performance of the Bayesian and SVM-based methods are sensitive to the training set.

REFERENCES

[1] M. Chamanbaz, E. Keikha, A. Mamunb, and Q. Wang, "Design of a probabilistic robust track-following controller for hard disk drive servo systems, " Mechatronics, vol. 24, Issue. 6, pp. 582-589, Sep 2014.

[2] Z. Chow, M.P. Ooi, Y. Kuang, and S. Demidenko, "Low-cost automatic visual inspection system for media in hard disk drive mass production," Instrumentation and Measurement Technology Conference (I2MTC), Austria, May. 2012, pp. 234-239.

[3] C. W. Mak, and N. V. Afzulpurkar, M. N. Dailey, and P. B. Saram, "A Bayesian approach to automated optical inspection for solder jet ball joint defects in the Head Gimbal Assembly process," *IEEE Trans. Automat. Sci. Eng.*, vol. PP, Issue. 99, Feb. 2014.

[4] Ieamsaard, J., & Fuangpian, T. Automated Optical Inspection for Solder Jet Ball Joint Defects in the Head Gimbal Assembly Process. *Visual Inspection Technology in the Hard Disk Drive Industry*, 99-129.

[5] N. Otsu, "A threshold selection method from gray-level histograms," *IEEE Trans. Syst., Man, Cybern.*, vol. 9, no. 1, pp. 62–66, Jan. 1979.

[6] S. Yammen, and P. Muneesawang, "An Advanced Vision System for the Automatic Inspection of Corrosions on Pole Tips in Hard Disk Drives," *IEEE Trans. Compon. Packag. Manuf. Technol.*, Jul. 2014.

[7] P. Liang, X. Zhiwei, and D. Jiguang, "Fast normalized cross-correlation image matching based on multiscale edge information," in *Proc. Int. Conf. Comput. Appl. Syst. Model. (ICCASM)*, Fuxin, China, pp. 507–511, Oct. 2010

[8] C. Chang, T. Chao, J. Horng, C. Lu, and R. Yeh, "Development pattern recognition model for the classification of circuit probe wafer maps on semiconductors," *IEEE Trans. Compon. Packag. Manuf. Technol.*, vol. 2, Issue: 12, pp. 2089 - 2097, Dec. 2012.

[9] H. Rhody, "Lecture 10: Hough circle transform," Chester F. Carlson Center for Imaging Science, October 11, 2005.

[10] P. Filipczuk, T. Fevens, R. Monczak, "Computer-aided breast concer diagnosis based on the analysis of cytological images of fine needle biopsies," *IEEE trans. Medical Imaging*, vol. 32, no. 12 pp. 2169-2178, Dec. 2013

[11] A. O. Ok. “A new approach for the extraction of aboveground circular structures from near-nadir VHR satellite imagery,” *IEEE Geosci. Remote Sens. Mag*., vol. 52, no. 6, Jun. 2014.
[12] W. Withayachumnankul, P. Kunakornvong, C. Asavathongkul, and P. Sooraksa, “Rapid detection of hairline cracks on the surface of piezoelectric ceramics,” *Int. J. Adv. Manuf. Technol.*, vol. 64, Issue: 9-12, pp.1275–1283, Feb. 2013.
[13] A. M. Al-Ghaili, S. Mashohor, A. R. Ramli, and A. Ismail, “Vertical-Edge-Based Car-License-Plate Detection Method,” *IEEE Trans. Veh. Technol*. vol. 62, Issue: 1, pp. 26 - 38, Jan. 2013.
[14] A. M. Al-Ghaili, S. Mashohor, A. Ismail, and A. R. Ramli, “A new vertical edge detection algorithm and its application,” in *Proc. Int. Conf. Comput. Eng. & Syst*. (ICCES), Egypt, Nov. 2008, pp. 204 – 209.
[15] X Liu, and J. Tang, “Mass classification in mammograms Using selected geometry and texture features, and a New SVM-Based feature selection method,” Systems Journal, IEEE, volume:8, Issue: 3, pp. 910-920, Nov. 2013.
[16] X. Gao, T. Lu, P. Liu, and Q. Lu, “A soil moisture classification model based on SVM used in agricultural WSN,” in *Proc*. Information Technology and Artificial Intelligence Conference *(ITAIC), IEEE 7th* Joint International, Dec. 2014, pp. 432-436.
[17] T. Barbu, “SVM-based human cell detection technique using histograms of oriented gradients,” in *Proc. 17th WSEAS* International Conference on Applied Mathematics *(AMATH ‘12),* Switzerland, 2012, pp. 156-160.
[18] J. Han and M. Kamber, *Data Mining: Concepts and Techniques*.San Francisco, CA, USA: Morgan Kaufmann, 2006, pp. 361-362.
[19] P. Kunakornvong, C. Tangkongkiet, and P. Sooraksa, “Defect Detection on Air Bearing Surface with Luminance Intensity Invariance,” *Proceeding of 9th International Conference on Fuzzy Systems and Knowledge Discovery (FSKD)*, pp. 693 – 696, 2012.
[20] Fak-aim, M., A. Seanton, and S. Kaitwanidvilai. "Automatic visual inspection of bump in flip chip using edge detection with genetic algorithm." *Proceedings of the International Multiconference of Engineers and Computer Scientists 2008*. 2008.
[21] Chow, Z. S., Ooi, M. P. L., Kuang, Y. C., & Demidenko, S. (2012). “Automated visual inspection system for mass production of hard disk drive media” .*Procedia Engineering*, *41*, 450-457.
[22] Gulphanich, S., N. Nunak, and T. Suesut. "3D Inspection for HDD Production Process using Laser Light Sectioning." *Proceedings of the International MultiConference of Engineers and Computer Scientists*. Vol. 1. 2015.
[23] Huang, S, and Pan Y. "Automated visual inspection in the semiconductor industry: A survey." *Computers in Industry* 66 (2015): 1-10.
[24] Shankar, N. G., Z. W. Zhong, and N. Ravi. "Classification of defects on semiconductor wafers using priority rules." *Defect and Diffusion Forum*. Vol. 230. 2004.
[25] Zontak, M, and Cohen I. "Defect detection in patterned wafers using anisotropic kernels." *Machine Vision and Applications* 21.2 (2010): 129-141.
[26] Tsai, D, and Luo J. "Mean shift-based defect detection in multicrystalline solar wafer surfaces." *Industrial Informatics, IEEE Transactions on* 7.1 (2011): 125-135.
[27] Yuan, T, Way K, and Suk J B. "Detection of spatial defect patterns generated in semiconductor fabrication processes." *Semiconductor Manufacturing, IEEE Transactions on* 24.3 (2011): 392-403.